ELECTRONIC SUPPLEMENTARY INFORMATION (ESI)

Reversible optical control of magnetism in engineered artificial multiferroics

Diego A. Ochoa,[a], Enric Menéndez,[b], Jesús López-Sánchez,[c] Adolfo Del Campo,[c] Zheng Ma,[b] Irena Spasojević,[b] Ignasi Fina,[d] José F. Fernández,[c] Fernando Rubio-Marcos,*[c] Jordi Sort*[be] and José E. García*[a]

[a] *Department of Physics, Universitat Politècnica de Catalunya - BarcelonaTech, 08034 Barcelona, Spain*

[b] *Department of Physics, Universitat Autònoma de Barcelona, 08193 Bellaterra, Spain*

[c] *Department of Electroceramics, Instituto de Cerámica y Vidrio - CSIC, 28049 Madrid, Spain*

[d] *Institut de Ciència de Materials de Barcelona (ICMAB-CSIC),08193, Barcelona, Spain*

[e] *Institució Catalana de Recerca i Estudis Avançats (ICREA), 08010 Barcelona, Spain*

** e-mail: frmarcos@icv.csic.es, jordi.sort@uab.cat; jose.eduardo.garcia@upc.edu*

S1 Characterization of the in-plane isotropic $Fe_{75}Al_{25}/BaTiO_3$ heterostructure

In-depth scrutiny of the ferroelectric domains inherent to an in-plane isotropic $Fe_{75}Al_{25}/BaTiO_3$ heterostructure has been undertaken by using confocal Raman microscopy (CRM) within a coherent experimental framework. This approach has unveiled explicit and discernible correlations between the isotropic alignment of the in-plane domain walls of the (100)-BTO crystal and the photo-induced activation stemming from ferroelectric domain switching. Fig. S1a shows an optical representation of the $Fe_{75}Al_{25}$ thin film that has been deposited onto the BTO crystal surface. The subsequent Raman visualizations, both on the surface (Fig. S1b-c) and the cross-

section (Fig. S1d), elucidate a domain configuration encompassing *a*-domains (red domains) and *c*-domains (blue domains). The crux of the domain architecture predominantly comprises 90° domain walls, culminating in striped regions oriented at 45° with respect to the sample's edges. The domain width exhibits non-periodic variations between adjacent domains, as evidenced in Fig. S1e and f.

While both FeAl/BTO heterostructures do share certain commonalities—namely, the possession of the same two ferroelectric domain types—their disparities are pronounced. A conspicuous morphological differentiation emerges from CRM observations: (i) the (100) BTO crystal showcases an even distribution of *a*-domains and *c*-domains, each constituting approximately 50% (as outlined in Fig. S1g). In contrast, the (001) BTO crystal reveals an uneven domain distribution, characterized by a predominance of out-of-plane domains (as evident in Fig. 1c and d of the main manuscript). Fig. S1h shows an illustrative 2D scheme to portray the domains arrangement of the (100) BTO crystal derived from the CRM observations.

The exploration into the light-induced macroscopic strain within the FeAl/(100)-BTO heterostructure, distinguished by the isotropic alignment of in-plane domain walls, lays the groundwork for highlighting the discernible magnetic property differences observed in the FeAl/(001)-BTO heterostructure. The measurements reveal elongations of approximately 100 nm and 60 nm in perpendicular directions (Fig. S1i). It is important to note that the local deformations are partially mitigated within an isotropic ferroelectric domain wall arrangement, whereas a substantial anisotropic light-induced strain is displayed when the domain walls are purposefully anisotropically oriented (as depicted in Fig. 2a and b of the main manuscript). Fig. S1j and k show the in-plane magnetic characterization $Fe_{75}Al_{25}/BaTiO_3$ heterostructure with an almost isotropic ferroelectric domain configuration.

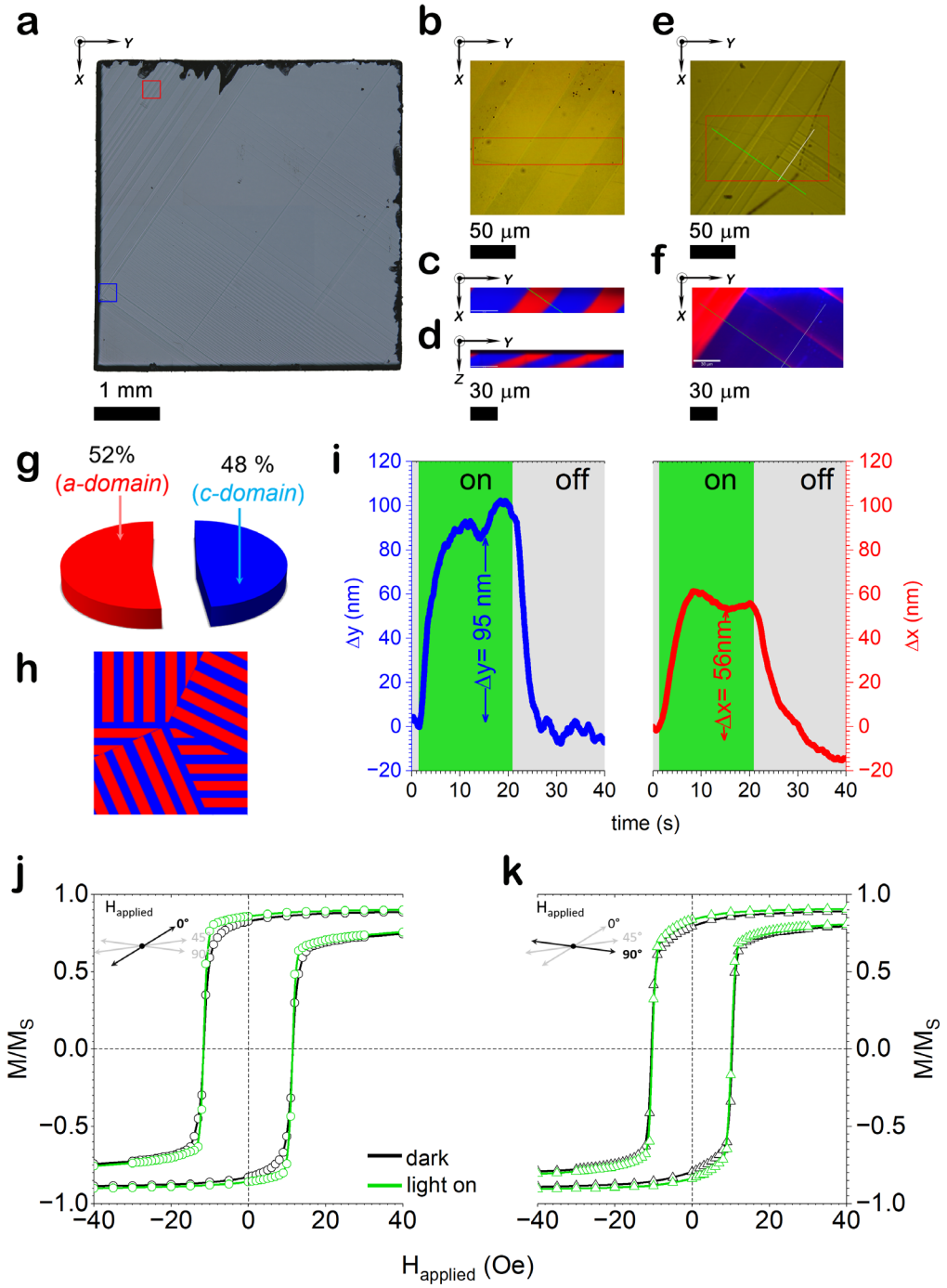

Fig. S1 Characterization of a $Fe_{75}Al_{25}/BaTiO_3$ heterostructure with an almost isotropic ferroelectric domain configuration. (a) Optical image of the sample surface showing a complex in-plane domain structure**.** (b) High-resolution optical image of the sample surface area marked with a red square in panel **a**. A regular domain pattern is observed. (c-d) Domain mapping corresponding to the area marked off by a red rectangle in panel **b**. The Raman images resulted from the collected single depth-scan Raman spectra of each *x,y,z* pixel of the selected area. Raman spectra with the same spectral shift for the Raman modes are identified using the same colour; that is, red for *a*-domains (in-plane) and blue for *c*-domain (out-of-plane). (e) High-resolution optical image of the sample surface area marked with a blue square in panel (a). (f) Domain mapping corresponding to the surface of the area marked off by a red rectangle in panel (e). (g) Domains distribution roughly estimated from a set of domain mapping (not shown) at representative areas of the sample. (h) Schematic representation of the $BaTiO_3$ domain pattern. (i) Light-induced macroscopic deformation of the sample in both *x* and *y* directions, according to panel (a). (j-k) Hysteresis loops with and without illumination with the magnetic field applied along both *x* and *y* directions, according to panel (a).

S2 Light control of strain in the $Fe_{75}Al_{25}/BaTiO_3$ heterostructure

The manipulation of visible-light-induced deformation within the FeAl/BTO heterostructure has significant implications for controlling its light-induced strain response. To investigate this aspect, a series of experiments has been undertaken to assess the relationship between deformation and light power in the direction perpendicular to the arrangement of domain walls. The outcomes of these experiments are detailed in Fig. S2. Notably, these foundational experiments affirm the capacity to systematically modulate light-induced strain through controlled variations in light power. The observed correlation depicts a linear trend between deformation, oriented perpendicularly to the arrangement of domain walls, and the applied light power across the examined range. Importantly, this phenomenon appears to lack a discernible light power threshold, further bolstering the proposition that engineered multiferroic materials hold promise as active optical components for systems requiring substantial anisotropic strain.

The light-induced effect engenders a reversible strain response, resulting in a substantial deformation of approximately 200 nm under a light power of 50 mW. This measured response aligns harmoniously with the macroscopic findings showcased in Fig. 2a of the main manuscript.

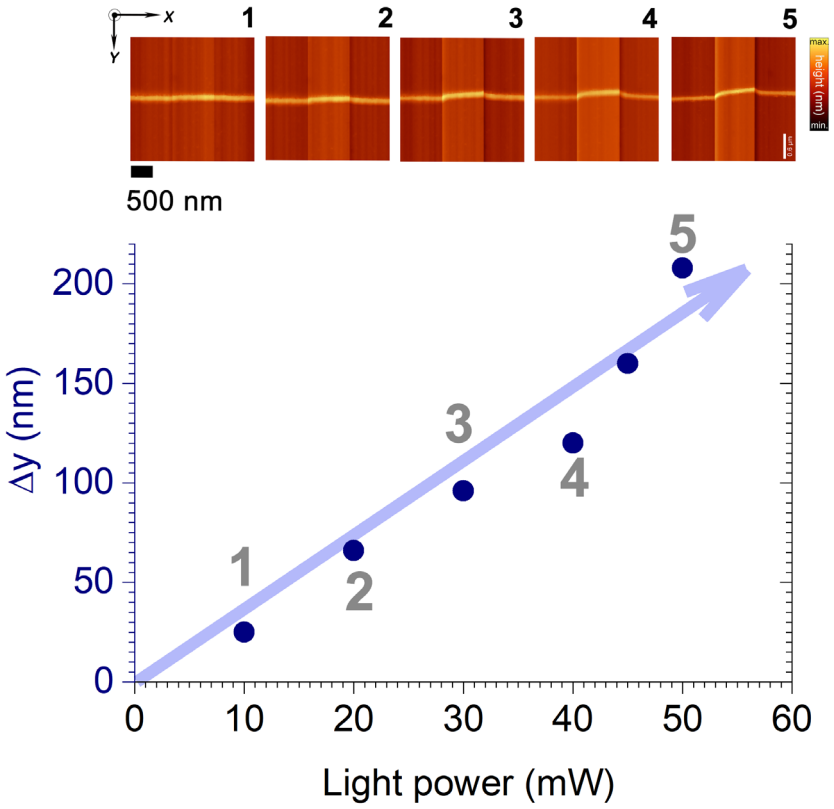

Fig. S2 Light-power dependence of in-plane strain. Light-induced local deformations within the FeAl/BTO artificial multiferroic are examined as a function of light power. The deformations occur perpendicularly to the BTO domain stripes. To investigate this phenomenon, a gold line arrangement was lithographically patterned onto the surface of the sample. The y-direction corresponds to the direction orthogonal to the BTO domain walls. At the upper part of the panel, a sequence of atomic force microscopy (AFM) topographic images showcases the stepwise scans of an off-on-off illumination cycle at various light powers. This sequence focuses on a region demarcated in Fig. 2e of the main manuscript, illustrating the pre-illumination and post-illumination positions of the gold line. The lower part of the figure depicts the evolution of in-plane deformation relative to the light power. Adjacent to the AFM images, numerical values delineate the corresponding light power settings.

S3 Power dependence and reversibility of the optical modulation

As seen in Fig. S3, light intensity dependence and reversibility were investigated. A clear light power dependence is observed and full reversibility is obtained once the system is back to non-illumination.

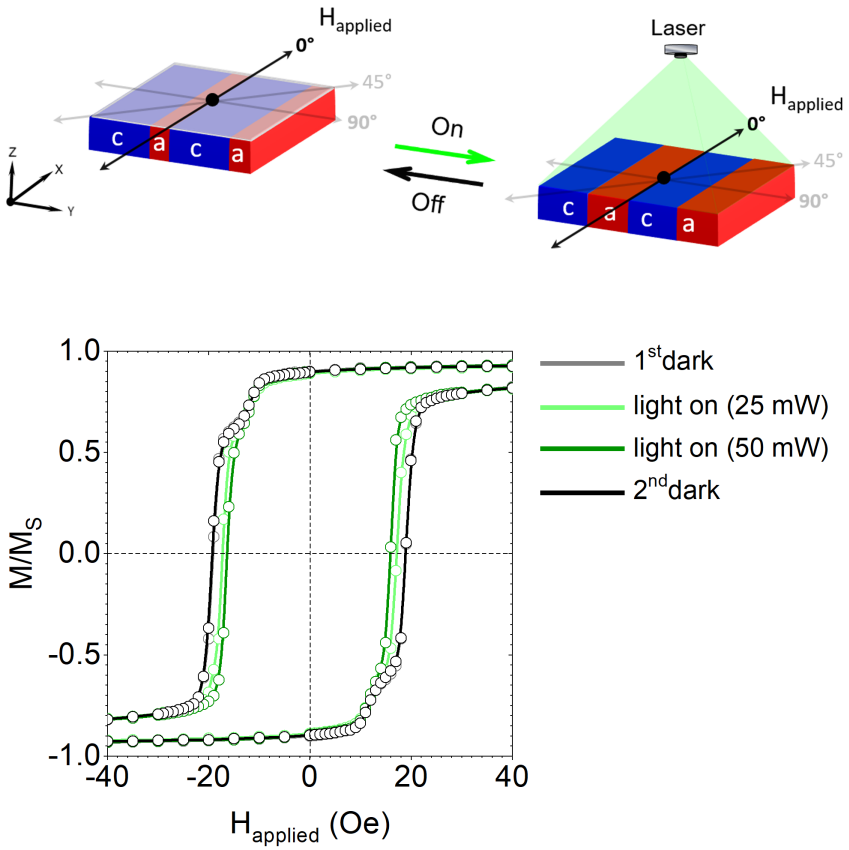

Fig. S3 Power dependence and reversibility of the optical modulation. Consecutive hysteresis loops along the FeAl lines taken in the following order: first without illumination, then with light to a power of 25 mW, with light to a power of 50 mW, and finally without illumination again.

S4 Magnetic response of $Fe_{75}Al_{25}/SiO_2/Si$ and $Fe_{75}Al_{25}$/PMN-PT heterostructures

To rule out the heating-induced effect in this optical modulation of magnetism, the FeAl film was grown atop a 300 nm SiO_2/0.5 mm [100]-oriented Si substrate (which has no piezoelectricity and, thus, no possibility to transfer strain to the ferromagnetic counterpart). Fig. S4a shows that this system exhibits no changes in magnetic behaviour with and without illumination, thus confirming that thermal effect is not the core of the observed optical modulation of magnetism in the $Fe_{75}Al_{25}/BaTiO_3$ heterostructure.

In addition, the FeAl film was also grown atop a 0.5 mm thick [110]-oriented $Pb(Mg_{1/3}Nb_{2/3})O_3$-$32PbTiO_3$ (PMN-PT) single crystal (with large piezoelectricity). Fig. S4b shows that this system exhibits no changes in magnetic behaviour with and without illumination, thus evidencing that visible-light- and electric-field-induced phenomena are not directly related.

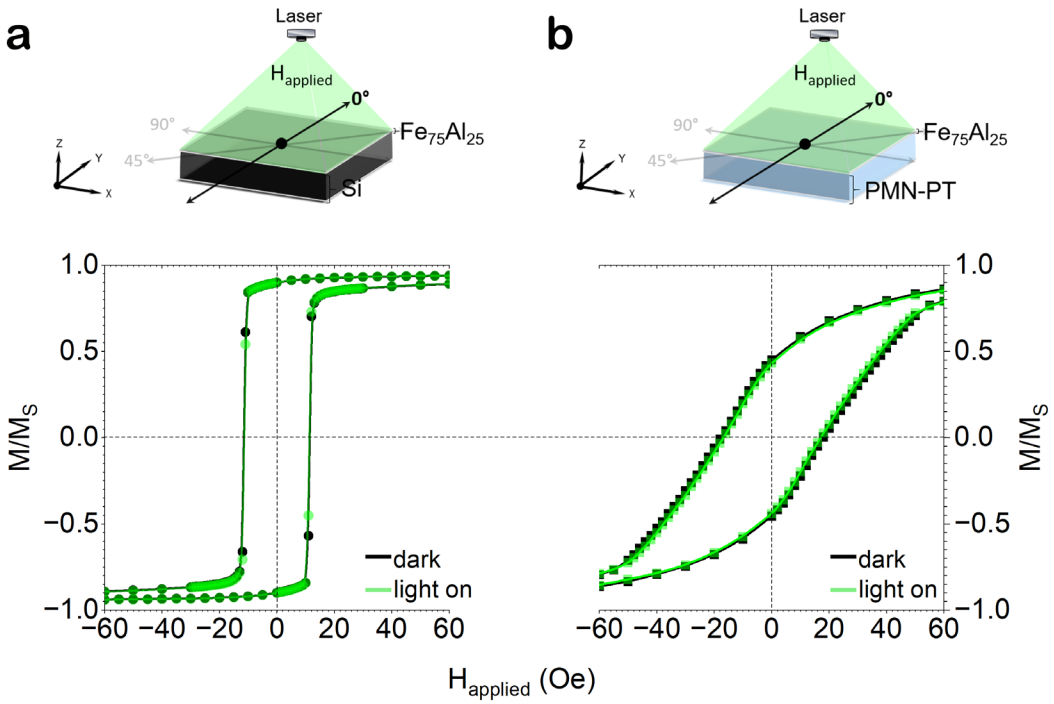

Fig. S4 Absence of optical modulation of magnetism in FeAl films grown atop SiO_2/Si substrates as well as FeAl/[110]-oriented PMN-PT. (a) Hysteresis loops with and without illumination of FeAl/SiO/Si heterostructure. (b) Hysteresis loops with and without illumination of FeAl/[110]-oriented PMN-PT heterostructure.